Multiphoton gradient index endoscopy for evaluation of diseased human prostatic tissue *ex vivo*

David M. Huland
Manu Jain
Dimitre G. Ouzounov
Brian D. Robinson
Diana S. Harya
Maria M. Shevchuk
Paras Singhal
Chris Xu
Ashutosh K. Tewari

Multiphoton gradient index endoscopy for evaluation of diseased human prostatic tissue *ex vivo*

David M. Huland,[a,*,†] **Manu Jain,**[b,†] **Dimitre G. Ouzounov,**[a] **Brian D. Robinson,**[c] **Diana S. Harya,**[d]
Maria M. Shevchuk,[c] **Paras Singhal,**[b] **Chris Xu,**[a] **and Ashutosh K. Tewari**[b]
[a]Cornell University, School of Applied and Engineering Physics, Ithaca, New York 14853, United States
[b]New York-Presbyterian Hospital, Department of Urology of Weill Medical College of Cornell University, New York 10021, United States
[c]New York-Presbyterian Hospital, Department of Surgical Pathology of Weill Medical College of Cornell University, New York 10021, United States
[d]Cornell University, College of Veterinary Medicine, Ithaca, New York 14853, United States

Abstract. Multiphoton microscopy can instantly visualize cellular details in unstained tissues. Multiphoton probes with clinical potential have been developed. This study evaluates the suitability of multiphoton gradient index (GRIN) endoscopy as a diagnostic tool for prostatic tissue. A portable and compact multiphoton endoscope based on a 1-mm diameter, 8-cm length GRIN lens system probe was used. Fresh *ex vivo* samples were obtained from 14 radical prostatectomy patients and benign and malignant areas were imaged and correlated with subsequent H&E sections. Multiphoton GRIN endoscopy images of unfixed and unprocessed prostate tissue at a subcellular resolution are presented. We note several differences and identifying features of benign versus low-grade versus high-grade tumors and are able to identify periprostatic tissues such as adipocytes, periprostatic nerves, and blood vessels. Multiphoton GRIN endoscopy can be used to identify both benign and malignant lesions in *ex vivo* human prostate tissue and may be a valuable diagnostic tool for real-time visualization of suspicious areas of the prostate. © The Authors. Published by SPIE under a Creative Commons Attribution 3.0 Unported License. Distribution or reproduction of this work in whole or in part requires full attribution of the original publication, including its DOI. [DOI: 10.1117/1.JBO.19.11.116011]

Keywords: multiphoton endoscopy; prostate cancer; optical histology; two-photon microscopy; second-harmonic generation.

Paper 140511R received Aug. 7, 2014; accepted for publication Oct. 24, 2014; published online Nov. 21, 2014.

1 Introduction

Prostate cancer remains the most commonly diagnosed cancer in U.S men with a projected 233,000 new diagnoses in 2014.[1] While a projected 29,480 men will die of prostate cancer in 2014, the majority have indolent cancer that may be less likely to progress or cause death. Identifying these patients is difficult with current diagnostic techniques. The Gleason score, which is obtained on biopsy, is by far the best predictor of cancer progression.[2] However, as only a fraction of the prostate gland is sampled and mostly in a blinded manner, prostate biopsies are only successful in detecting tumors in 60% to 70% of cases.[3] In prostates removed by radical prostatectomy (RP), an upstaging (>T2) is seen in 20.6% cases and an upgrading (Gleason score >6) in 44.9% cases was found on final histopathology.[4] As a consequence of such inaccuracies in staging and grading prostate cancer (Pca), nonindolent cancer candidates are often put under active surveillance (AS) leading to cancer progression. Furthermore, many suitable candidates are not enrolled in AS and receive unnecessary overtreatment with concomitant side effects.

RP is the frequently selected treatment option for men with localized prostate cancer. However, a significant challenge faced by surgeons during RP is the complete removal of the cancerous tissue, while preserving the nerves surrounding the prostate that are responsible for continence and erectile function. These nerves, as well as the malignant glands, are too small to be visualized by the human eye. Although RP with the da Vinci robotic

surgical system allows for a significant advantage in surgical precision due to 10 to 12× magnification of the surgical field, it lacks the cellular resolution to differentiate cancerous cells from surrounding nerve tissue. Thus, some surgeons rely on intraoperative frozen section (IFS) analysis to provide some benefit in reducing positive surgical margins (PSMs).[5] However, frozen sections require time and only provide an assessment of a fraction of the area of interest. Further, as IFS requires the removal of tissue, there is still a risk of damaging the area one is trying to preserve, especially the periprostatic nerves. RPs have PSMs[6] in 13.8% to 22.8% of cases and a 6% to 27% rate of postoperative impotence.[7] In essence, inaccurate disease quantification, staging, and unavailability of intraoperative pathological guidance often result in mismatched treatment recommendations, overtreatment, residual cancer (positive surgical margins) during surgery, and the need for expensive radiation treatment to salvage these cancers. Thus, for both the diagnosis and the treatment of prostate cancer, a faster and more accurate way of characterizing the tissue at a cellular level could significantly improve decision making during treatment and patient outcomes.

Multiphoton microscopy (MPM) provides the ability to image fresh, unprocessed (unstained and unfixed) tissues at subcellular resolution *in vivo*.[8–10] It has been demonstrated to provide tissue architecture comparable to gold standard H&E and has been shown as a valuable tool in the diagnosis of benign and malignant lesions in multiple organs including the lung,[11,12] bladder,[13] and ovaries.[14] Its ability to image unprocessed and unstained human prostate tissues, *ex vivo* has further shown that MPM can identify relevant prostatic and periprostatic tissues and pathological changes.[15,16] Although these studies

*Address all correspondence to: David M. Huland, E-mail: dmh56@cornell.edu

†These authors contributed equally.

serve as a baseline to establish the signature of the various tissue types and pathologies on MPM, the bench top MPM microscope used in these studies cannot be used *in vivo* intraoperatively.

We have previously reported on a compact and portable gradient index (GRIN)-based endoscope for clinical multiphoton applications.[17,18] The design of this device is centered around a rigid 8-cm length, 1-mm diameter GRIN endoscopic probe and can image a 200-μm diameter field of view (FOV) at 4 fps (512×512 pixels) at a subcellular resolution. The small diameter of this device could allow it to be used inside a needle to inspect and to identify suspicious tissue sites. We have demonstrated the device through *in vivo* imaging of the kidney, colon, and liver in anesthetized rats. In this study, we test the diagnostic capabilities of our GRIN endoscope on *ex vivo* human prostate samples obtained from radical prostatectomy patients.

2 Materials and Methods

2.1 Portable and Compact GRIN Endoscope System

The compact and portable GRIN endoscope system is shown in Fig. 1 and was previously described.[17,18] In brief, the near-infrared excitation pulses are delivered to the device via a ∼2-m hollow core photonic band-gap fiber. After being collimated by an aspheric lens on the portable GRIN lens endoscope, the beam is scanned by a two-axis galvanometer scan mirror system, and two scan lenses and a 0.3 NA objective are used to scan the back of the GRIN lens endoscope system. This is composed of a 0.1 NA relay lens (1.75 pitch) and a 0.5 NA objective lens (<0.25 pitch). The GRIN probe is 1 mm in diameter and has a thin protective metal casing, which may help to puncture tissue, for a total outer diameter of 1.2 mm. For the *ex vivo* human tissue demonstration at Weill Cornell Medical Center we used a turn-key, compact fiber laser system at 780 nm with a repetition rate of 50 MHz (Carmel, Calmar Laser). Due to the shifted wavelength closer to the zero dispersion wavelength of the fiber as compared to our previous demonstration at 800 nm,[17] we were able to remove the piece of dispersive glass previously used for dispersion compensation, yielding a pulse width of ∼150 fs at the sample. The fluorescence signal from the sample is epicollected through the GRIN system and the microscope objective, and is reflected by two dichroic beam splitters and

collected into two different channels for autofluorescence (∼405 to 700 nm) and second-harmonic generation (SHG) (<405 nm). The resulting system weighs less than 2 lbs and can image a 200-μm diameter FOV at 4 fps (512×512 pixels) at a subcellular resolution. Resulting images were postprocessed to improve contrast and brightness levels and pseudocolored with autofluorescence in green and SHG in red.

2.2 Ex Vivo Human Prostate Imaging

The present study included 14 robotic radical prostatectomies from patients who agreed to participate in an Institutional Review Board approved study. Patients ranged in age from 41 to 75 years. Prostates removed by RP were first taken to the Department of Surgical Pathology for gross examination. One specimen was immediately imaged intact after RP to identify periprostatic tissue. For the rest of the 13 specimens, surfaces were inked as per institutional protocol, and then specimens were roughly sliced in 0.5-cm-thick sections. One section per specimen with visible tumor or most likely to have tumor was chosen by a uropathologist. The sections were brought to the multiphoton endoscopy facility in normal saline and imaged at room temperature with the GRIN endoscope. All the sections were imaged under the guidance of a research pathologist experienced with MPM imaging. Images were acquired from areas labeled as benign and malignant on gross inspection of the section. Unless otherwise noted, all samples were imaged within ∼3 h of excision from the patient, and at 50 mW at the sample and at 4 fps. The imaging software MPScan[19] was instantly used to process pseudo color and display images. Additional contrast and brightness processing was done in the images in Figs. 2–4 to highlight any visible features. During imaging, the sample was fixed in agar gel to reduce motion artifacts. 0.9% phosphate buffered saline was used for GRIN objective immersion and to prevent the tissue from drying out. Throughout the imaging sessions, the portable GRIN endoscope was mounted on a three-dimensional stage for fine movement control. After imaging, the specimen was returned to the Department of Surgical Pathology in 10% buffered formalin and processed for routine histopathology (formalin fixation, embedding, sectioning, and staining). All H&E images shown in the figures were taken under an oil immersion objective (100X) with a total magnification of 1000× to match the FOV of ∼150×150 μm^2 on the MPM. H&E comparison images were taken from the same
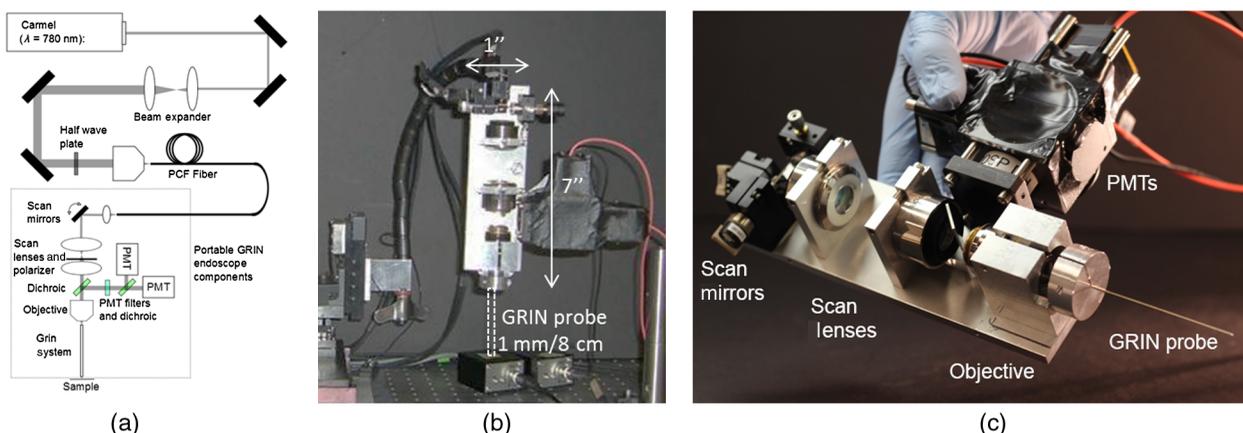
Fig. 1 Portable GRIN endoscope. (a) Optical drawing and (b) photograph of the GRIN-based endoscope system as mounted for imaging and (c) close up of the portable GRIN endoscope.
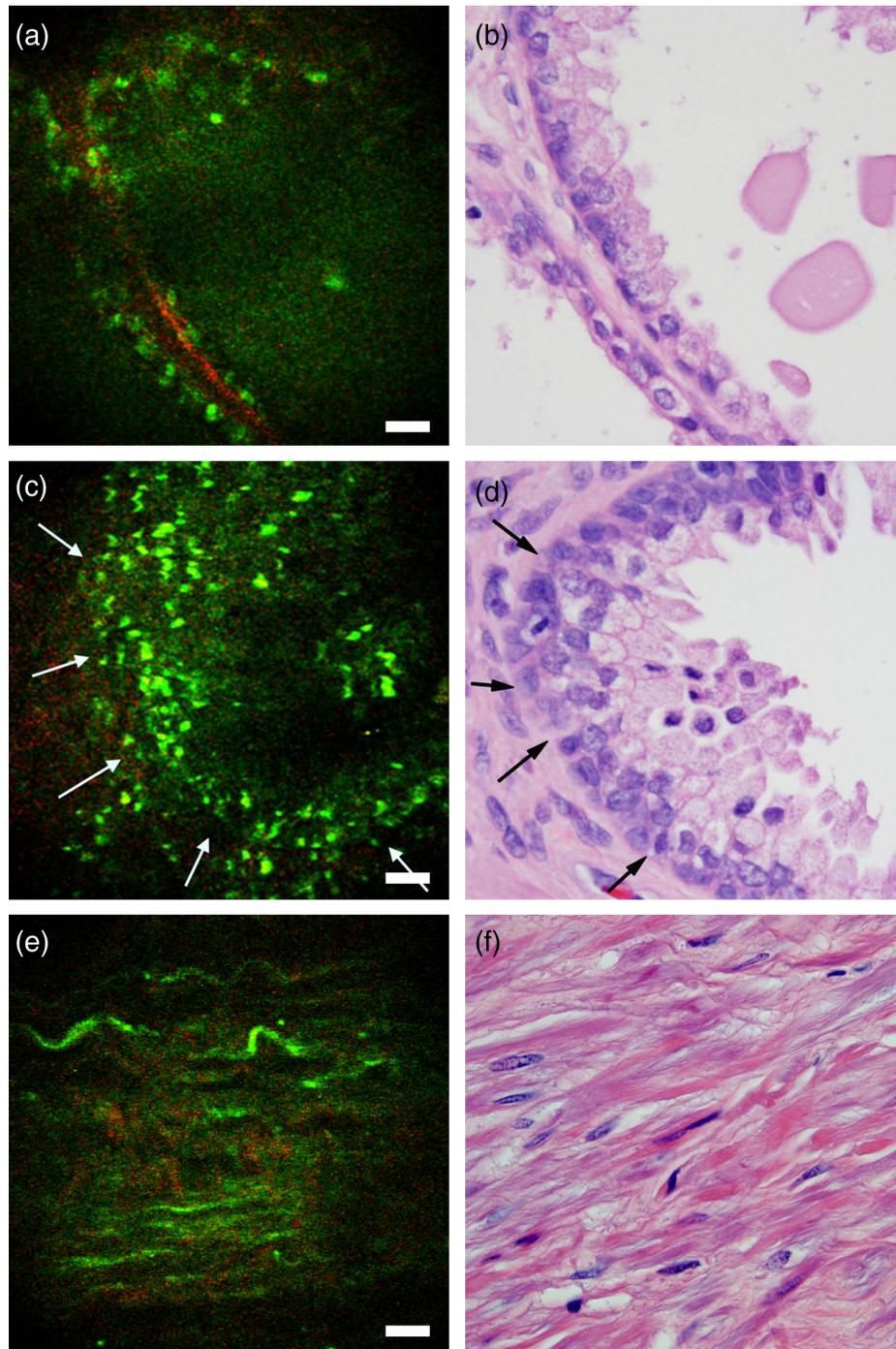
Fig. 2 *Ex vivo* imaging of benign prostatic tissue. (a,c) Multiphoton endoscopy images of benign prostatic glands (arrows) with (a) flat epithelium along with secretion/concretions and (c) infolded epithelium and ruffled luminal border in the lumen. (e) Multiphoton endoscopy image of stroma. Scale bars are 20 μm (b, d, f) corresponding H&E stained sections. H&E: Total magnification = 1000×.

sample and from a similar area of the site where the original multiphoton endoscopy image was taken.

3 Results

3.1 Imaging of the Prostate Gland

The prostate gland is mainly composed of two components: acini and fibromuscular stroma. In the multiphoton endoscopy images of the benign prostatic tissue (Fig. 2), we could identify benign glands based on their architecture, i.e., large gland with infolded epithelium and ill-defined luminal border. In addition, strong punctate autofluorescence in the cytoplasm was uniquely seen in the benign glands. This signal most likely originates from lipofuscin found abundantly in the cytoplasm of the benign glands. Some benign glands were seen lined by flattened epithelium with secretions/concretions in their lumen. Similarly, the fibromusclar stroma had a strong SHG signal generated by collagen along with autofluorescent muscle fibers and some elastin fibers. By comparison, the images taken from areas
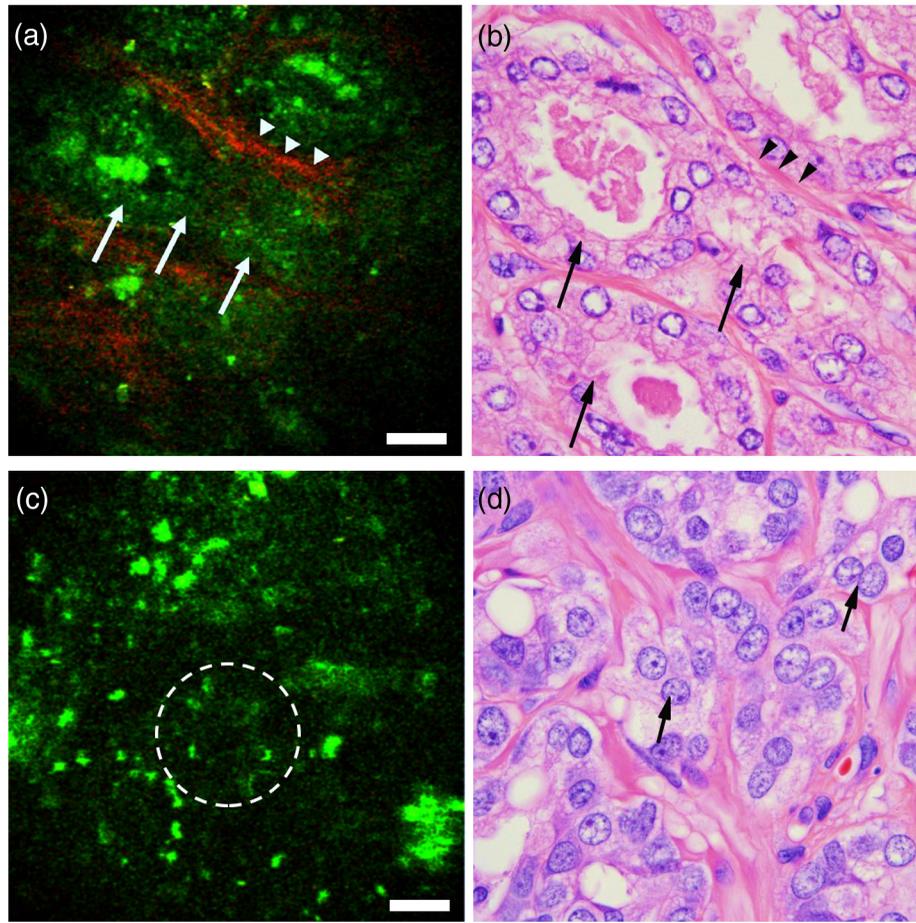
Fig. 3 *Ex vivo* imaging of prostate tumor. (a, c) Multiphoton endoscopy images of adenocarcinoma prostate showing (a) an example of a low-grade tumor area with clusters of tiny glands (arrows), separated by a thin band of collagen fibers (arrowheads) and (c) example of a high-grade tumor areas of irregularly shaped or poorly formed glands [circled area in (c) and arrows in (d)]. Scale bars are 20 μm. And (b, d) corresponding H&E images. H&E: Total magnification = 1000×.

with adenocarcinoma (Fig. 3) showed clusters of small acini with sharp luminal borders and some aggregated small secretions in the lumen. These areas were confirmed to have low-grade tumor (Gleason $3 + 3 = 6$) on H&E. In the areas confirmed as high grade (Gleason 7+) adenocarcinoma on H&E, MPM images showed loss of normal architecture and it was challenging to identify individual acini. Furthermore, the SHG signal was significantly reduced in areas of high-grade tumor as compared to areas of low-grade tumor. In the images in Fig. 3, the average SHG signal of the top 10% of pixels was 39 (on a 0 to 255 scale) for Fig. 3(a) as compared to 12 (on a 0 to 255 scale) for Fig. 3(c).

3.2 *Imaging of Periprostatic Tissue*

In addition to imaging sections from the prostate glands, in one case we imaged the surface of an intact RP specimen to simulate intraoperative margin imaging. Here, we could identify relevant periprostatic tissues, such as adipocytes, periprostatic nerves, and blood vessels (Fig. 4). Adipocytes were recognized based on their globular shape and homogeneous cytoplasm. Nerve was clearly identified by its wavy nerve fibers and was distinguishable from blood vessel due to the lack of lumen.

Being able to obtain histologic quality images at lower excitation powers could be beneficial to reduce concerns about the safety of multiphoton endoscopy. In Fig. 5, we reduce the power to 32 mW while keeping the frame rate constant at 4 fps [Fig. 5(b)]. While the signal-to-noise ratio in the image is decreased, most of the architecture is still visible as compared to the original image at 50 mW. Similarly, if motion artifacts could be overcome to a point where longer integration times are not a problem, Fig. 5(e) shows that we can obtain images of very comparable quality at 6 mW excitation power when averaging 16 frames obtained at 1 fps (i.e., 16 s total acquisition time).

4 Discussions and Conclusions

We have demonstrated that multiphoton GRIN endoscopy can image fresh, unfixed and unprocessed prostate tissues at a sub-cellular resolution. We can not only identify but also differentiate areas with benign glands from areas with adenocarcinoma in *ex vivo* prostate sections. In addition, we identified important periprostatic tissues such as nerves, adipocytes, and blood vessels. This study demonstrates the feasibility and lays the foundation for future *in vivo* imaging in prostate cancer patients to improve their diagnosis and management.

Images obtained from the *in vivo* rat experiment demonstrate multiphoton GRIN endoscopy as a potential tool for *in vivo* imaging in human subjects intraoperatively. As we have
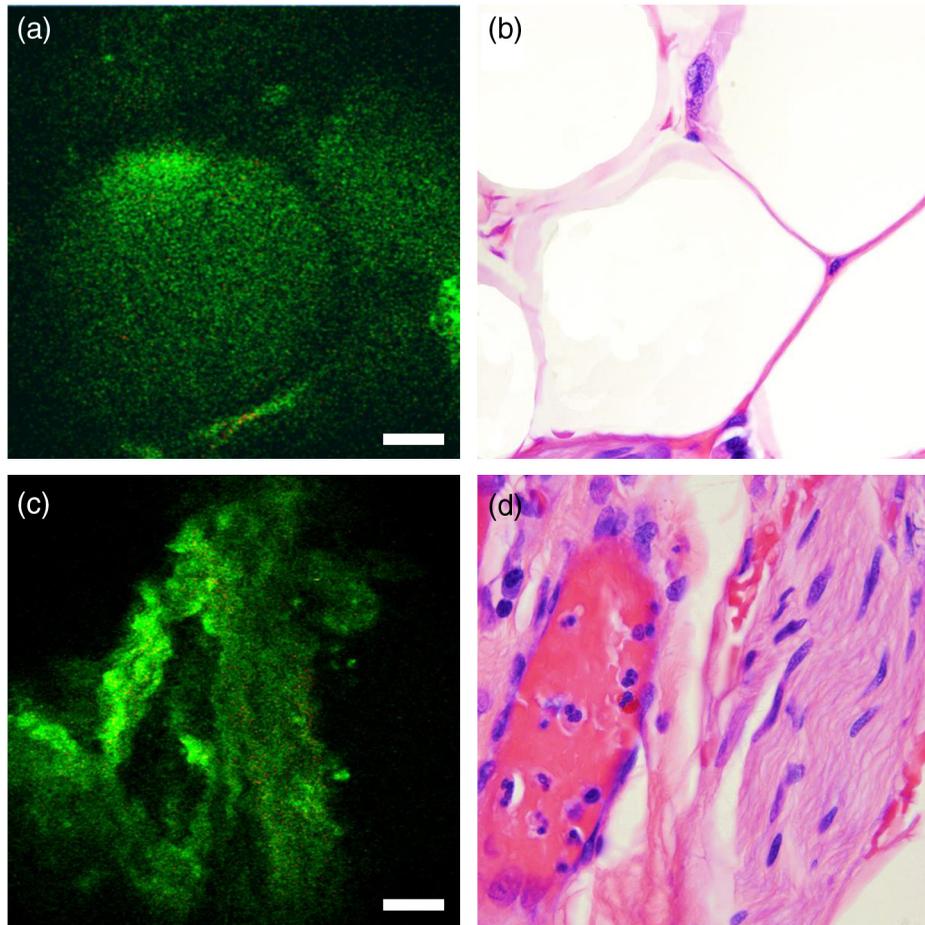
Fig. 4 *Ex vivo* imaging of periprostatic tissue. (a) Multiphoton endoscopy image of adipocytes, and (c) a neurovascular bundle. Scale bars are 20 μm. And (b,d) corresponding H&E images. H&E: Total magnification = 1000×.

previously described,[17] the main source of motion artifacts during *in vivo* rat experiments is movement from the diaphragm during respiration. While we were able to successfully isolate this motion during this demonstration, the exact effect of this on the quality of the images during surgery needs to be investigated. We would anticipate the respiratory motion to be less significant in human subjects due to a significantly slower respiratory rate and a considerable distance of the pelvis from the diaphragm. However, one could expect more contribution from cardiovascular motion in a human subject. The pneumoperitoneum created during robotic RP could help significantly in reducing the effect of both cardiac and pulmonary motion artifacts. Mounting the device on a flexible arm that can be tightened while taking an image as previously demonstrated on rats[17] will eliminate any motion artifacts from holding the device. Further, previous studies have successfully demonstrated dynamically stabilizing recording devices *in vivo* using piezo manipulators[20] and correcting for motion artifacts in postprocessing.[21,22]

The ultimate goal of multiphoton endoscopy is to achieve a real-time visualization of prostatic tissue in a clinical setting. Based on the images obtained in this study and the fact that this device is potentially compatible in dimensions (8-cm length× 1-mm diameter) with a biopsy needle, we envision its integration in the prostate biopsy gun to carry out targeted biopsies.

By achieving real-time histology, we can improve the diagnostic accuracy of the Gleason grading by increasing the yield of cancerous tissue (by sampling the suspicious area) for histopathological diagnosis during biopsy procedure. This can be a valuable tool for better selection of active surveillance patients and reduces the rates of under or overtreatment. This device could also be used intraoperatively during radical prostatectomy to identify periprostatic nerves and to assess surgical margins, potentially reducing complications associated with RP such as erectile dysfunction and urinary incontinence and resulting in improved functional outcomes and quality of life for the patients.

Before this endoscopic device can be integrated into routine clinical workflow, several potential challenges need to be addressed. The most significant one is probably proving that the excitation powers used are not harmful to the imaged tissue. We have shown that if motion artifacts could be significantly reduced, excitation powers as low as 6 mW would be sufficient for similar quality images. Additionally, several studies have suggested that the higher power levels used in this study are below the threshold for DNA and other tissue damage.[9,23] However, due to multiple factors potentially influencing these thresholds (including numerical aperture, wavelength, pulse width, aberrations in the optical system, and exposure time), the exact threshold needs to be characterized for the presented endoscope.
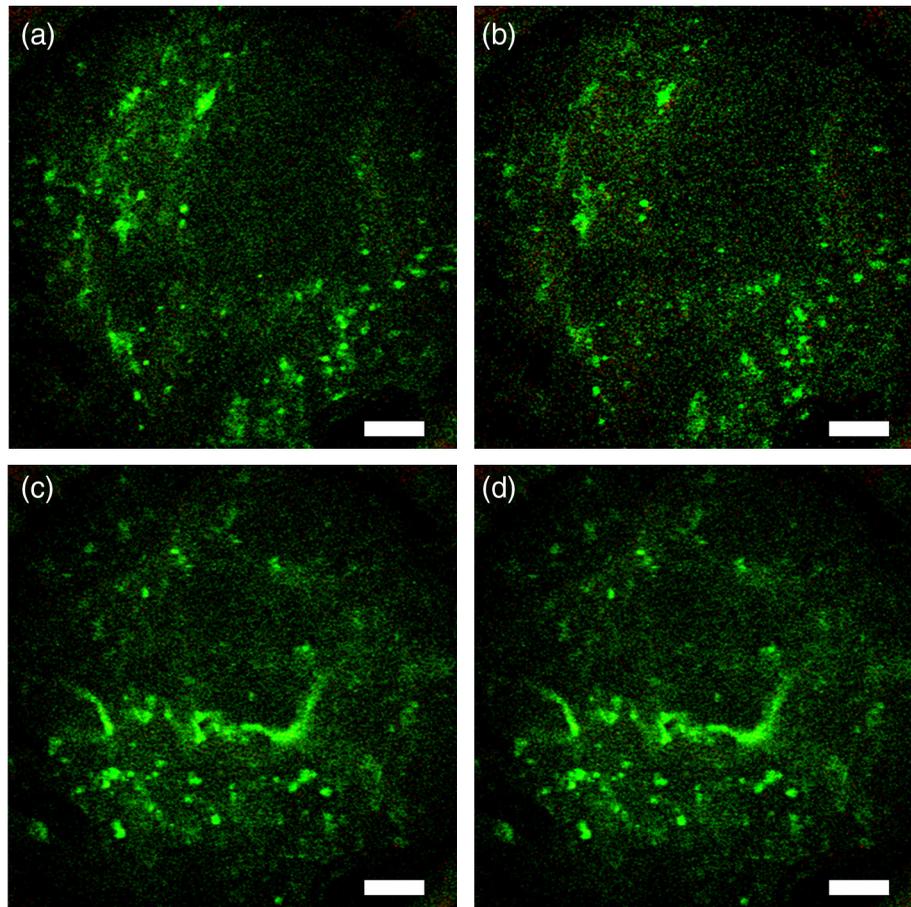
Fig. 5 *Ex vivo* human prostate imaging and averaging. (a,c) Multiphoton endoscopy images of prostate showing (a) a ~150 × 150 μm field-of-view (FOV) taken at 4 fps and 50-mW excitation power at the sample. (b) Frame rate kept constant at 4 fps and excitation power reduced to 32 mW. (d) Excitation power reduced to 6 mW and 16 frames averaged at 1 fps (i.e., 16 seconds per frame). Scale bars are 20 μm.

Further, the clinical environment may provide new challenges, such as cardiac motion and blood interfering with the imaging. The presented endoscope can image a 200-μm FOV at 4 fps. Motion artifacts could be overcome by increasing the frame rate further and strategies have been suggested to achieve this.[24] Challenges involving blood and other tissues interfering with the images could be overcome by adding the ability to flush the surface of the endoscope with saline. The major limitation from a diagnostic point of view is the very small FOV of 200 μm that limits the area under inspection and impedes architectural analysis. A larger FOV would be advantageous to scan a larger fraction of the prostate to give an idea of the overall architecture under imaging. At the cost of resolution, one could increase the FOV by decreasing the objective NA used. Although in our study, the FOV appeared sufficient to generally distinguish benign from malignant tissue and we were able to identify areas with low-grade and high-grade tumors, a larger sample size and further studies are needed to verify this claim.

In summary, we have shown that multiphoton GRIN endoscopy can be used to identify both benign and malignant lesions in *ex vivo* human prostate tissue. The GRIN endoscope is integrated into a compact and portable device that could potentially be used in a clinical setting for guided biopsies or intraoperative assessment of periprostatic nerves and prostatic margins. This may reduce complications associated with over or under treatment and improve functional outcomes and quality of life for prostate cancer patients.

References

1. R. Siegel et al., "Cancer statistics, 2014," *CA. Cancer J. Clin.* **64**(1), 9–29 (2014).
2. L. Cheng et al., "The combined percentage of Gleason patterns 4 and 5 is the best predictor of cancer progression after radical prostatectomy," *J. Clin. Oncol.* **23**(13), 2911–2917 (2005).
3. F. K.-H. Chun et al., "Optimizing performance and interpretation of prostate biopsy: a critical analysis of the literature," *Eur. Urol.* **58**(6), 851–864 (2010).

4. A. El Hajj et al., "Analysis of outcomes after radical prostatectomy in patients eligible for active surveillance (PRIAS)," *BJU Int.* **111**(1), 53–59 (2013).

5. W. Dillenburg et al., "Laparoscopic radical prostatectomy: the value of intraoperative frozen sections," *Eur. Urol.* **48**(4), 614–621 (2005).

6. P. Sooriakumaran et al., "A multinational, multi-institutional study comparing positive surgical margin rates among 22393 open, laparoscopic, and robot-assisted radical prostatectomy patients," *Eur. Urol.* **66**(3), 450–456 (2013).

7. V. Ficarra et al., "Systematic review and meta-analysis of studies reporting potency rates after robot-assisted radical prostatectomy," *Eur. Urol.* **62**(3), 418–430 (2012).

8. W. Denk, J. Strickler, and W. Webb, "Two-photon laser scanning fluorescence microscopy," *Science* **248**(4951), 73–76 (1990).

9. J. M. D. Cruz et al., "Feasibility of using multiphoton excited tissue autofluorescence for in vivo human histopathology," *Biomed. Opt. Express* **1**(5), 1320–1330 (2010).

10. W. R. Zipfel et al., "Live tissue intrinsic emission microscopy using multiphoton-excited native fluorescence and second harmonic generation," *Proc. Natl. Acad. Sci. U. S. A.* **100**(12), 7075–7080 (2003).

11. M. Jain et al., "Multiphoton microscopy: a potential 'optical biopsy' tool for real-time evaluation of lung tumors without the need for exogenous contrast agents," *Arch. Pathol. Lab. Med.* **138**(8), 1037–1047 (2013).

12. I. Pavlova et al., "Multiphoton microscopy and microspectroscopy for diagnostics of inflammatory and neoplastic lung," *J. Biomed. Opt.* **17**(3), 036014 (2012).

13. M. Jain et al., "Multiphoton microscopy in the evaluation of human bladder biopsies," *Arch. Pathol. Lab. Med.* **136**(5), 517–526 (2012).

14. R. M. Williams et al., "Strategies for high-resolution imaging of epithelial ovarian cancer by laparoscopic nonlinear microscopy," *Transl. Oncol.* **3**(3), 181–194 (2010).

15. A. K. Tewari et al., "Multiphoton microscopy for structure identification in human prostate and periprostatic tissue: implications in prostate cancer surgery," *BJU Int.* **108**(9), 1421–1429 (2011).

16. R. Yadav et al., "Multiphoton microscopy of prostate and periprostatic neural tissue: a promising imaging technique for improving nerve-sparing prostatectomy," *J. Endourol.* **23**(5), 861–867 (2009)..

17. D. M. Huland et al., "In vivo imaging of unstained tissues using long gradient index lens multiphoton endoscopic systems," *Biomed. Opt. Express* **3**(5), 1077–1085 (2012).

18. D. M. Huland et al., "Three-photon excited fluorescence imaging of unstained tissue using a GRIN lens endoscope," *Biomed. Opt. Express* **4**(5), 652–658 (2013).

19. Q.-T. Nguyen, P. S. Tsai, and D. Kleinfeld, "MPScope: a versatile software suite for multiphoton microscopy," *J. Neurosci. Methods* **156**(1–2), 351–359 (2006).

20. M. S. Fee, "Active stabilization of electrodes for intracellular recording in awake behaving animals," *Neuron* **27**(3), 461–468 (2000).

21. D. S. Greenberg and J. N. D. Kerr, "Automated correction of fast motion artifacts for two-photon imaging of awake animals," *J. Neurosci. Methods* **176**(1), 1–15 (2009).

22. D. A. Dombeck et al., "Imaging large-scale neural activity with cellular resolution in awake, mobile mice," *Neuron* **56**(1), 43–57 (2007).

23. R. Ramasamy et al., "Identification of spermatogenesis with multiphoton microscopy: an evaluation in a rodent model," *J. Urol.* **186**(6), 2487–2492 (2011).

24. D. R. Rivera et al., "Multifocal multiphoton endoscope," *Opt. Lett.* **37**(8), 1349–1351 (2012).

Biographies of the authors are not available.